Ann. Occup. Hyg., Vol. 55, No. 4, pp. 410–420, 2011

doi:10.1093/annhyg/meq091

Deriving Realistic Source Boundary Conditions for a CFD Simulation of Concentrations in Workroom Air

CHARLES E. FEIGLEY[1]*, THANH H. DO[2], JAMIL KHAN[2], EMILY LEE[1,3], NICHOLAS D. SCHNAUFER[1] and DEBORAH C. SALZBERG[1]

[1]Department of Environmental Health Sciences, Arnold School of Public Health, Room 401, University of South Carolina, 921 Assembly Street, Columbia, SC 29208, USA; [2]Department of Mechanical Engineering, Room A224, School of Engineering and Computing, University of South Carolina, 300 Main Street, Columbia, SC 29208, USA

Received 31 December 2009; in final form 28 October 2010; published online 21 March 2011

Computational fluid dynamics (CFD) is used increasingly to simulate the distribution of airborne contaminants in enclosed spaces for exposure assessment and control, but the importance of realistic boundary conditions is often not fully appreciated. In a workroom for manufacturing capacitors, full-shift samples for isoamyl acetate (IAA) were collected for 3 days at 16 locations, and velocities were measured at supply grills and at various points near the source. Then, velocity and concentration fields were simulated by 3-dimensional steady-state CFD using 295K tetrahedral cells, the k-ε turbulence model, standard wall function, and convergence criteria of 10^{-6} for all scalars. Here, we demonstrate the need to represent boundary conditions accurately, especially emission characteristics at the contaminant source, and to obtain good agreement between observations and CFD results. Emission rates for each day were determined from six concentrations measured in the near field and one upwind using an IAA mass balance. The emission was initially represented as undiluted IAA vapor, but the concentrations estimated using CFD differed greatly from the measured concentrations. A second set of simulations was performed using the same IAA emission rates but a more realistic representation of the source. This yielded good agreement with measured values. Paying particular attention to the region with highest worker exposure potential—within 1.3 m of the source center—the air speed and IAA concentrations estimated by CFD were not significantly different from the measured values ($P = 0.92$ and $P = 0.67$, respectively). Thus, careful consideration of source boundary conditions greatly improved agreement with the measured values.

Keywords: boundary conditions; computational fluid dynamics (CFD); emission rates; exposure estimation; far field; isoamyl acetate; near field

INTRODUCTION

The understanding of exposure to airborne contaminants in enclosed spaces is important for numerous applications, including exposure and risk assessment, exposure control, toxicology, and occupational epidemiology. Although reliable methods for monitoring exposures are available, exposures are directly measured for only a tiny fraction of workers. Thus, development and validation of other methods for exposure estimation are essential for protecting the workers' health.

Exposure estimation poses a significant challenge in enclosed spaces where the concentration varies

*Author to whom correspondence should be addressed. Tel: +1-803/777-6360; fax: +1-803/777-3391; e-mail: cfeigle@mailbox.sc.edu
[3]Present address: Exposure Assessment Branch, Health Effects Laboratory Division, National Institute for Occupational Safety and Health, 1095 Willowdale Road, Morgantown, WV 26505, USA.

with location. The spatial distribution of a contaminant is a complex function of many factors, including the characteristics of the room and of the contaminant. Deterministic modeling that explicitly accounts for the effects of factors that determine the concentration is one means of estimating concentration throughout a room. Computational fluid dynamics (CFD) accounts for a more comprehensive set of determining factors than the other deterministic approaches; hence, it is used extensively in simulating the motion of fluids and associated heat and mass transport.

Despite its considerable power and extensive use in predicting flow patterns for heating, ventilating, and air conditioning and indoor air engineering, CFD has been used only modestly for analyzing the distribution of airborne contaminants in workrooms with mixing ventilation. This is due to several factors, including the relatively small number of researchers working to validate CFD for this purpose, and the sensitivity of CFD solutions for mixed spaces to uncertainties in boundary characteristics: the former has led to a paucity of validation data sets from workrooms and the latter has made simulation of these data sets more challenging. CFD analysis of a workroom begins by establishing the boundaries that enclose the space to be modeled, called the 'computational domain'. These boundaries are either solid (e.g. walls, process equipment, and furniture) or open (e.g. windows, doors, supply air outlets, and hoods). The relevant characteristics of these boundaries, also known as boundary conditions, must be defined. The domain is divided into a network of small cells. The equations describing the conservation of mass, energy, and momentum for each cell comprise a large set of equations that is then solved numerically.

The treatment of boundaries in books on the fundamentals of CFD generally focuses on boundary layer flow in proximity to solid boundaries (e.g. Patankar, 1980; Anderson *et al.*, 1984). As shown in the following discussion, more recent papers have dealt with the importance of supply air fixtures. Small-scale determination of air velocity from supply inlets and representation of these details in CFD calculations were found to be essential for simulation of a scale model of a workroom with a wall jet air inlet (Lee and Feigley, 2002) and of an embalming room with a ceiling diffuser inlet (Bennett *et al.*, 2003). A survey on quality control of CFD for indoor environments concluded that the fine details of flow from an inlet diffuser must be addressed pointing out that the momentum of inlet jets from diffusers can impact airflow patterns throughout a room (Sorensen and Nielsen, 2003). The influence of uncertainties in supplying airflow rate and boundary temperatures on CFD estimates of heat and mass transport in ventilated spaces was investigated in detail (Teodosiu *et al.*, 2003). That study demonstrated that precise representation of supply inlets in CFD is vital for obtaining good agreement of calculated air velocities and temperatures with measured values for ventilated enclosures. Various approaches for incorporating these inlet flow details in CFD have also been reported (Nielsen, 2004). Recognizing the importance of the inlet boundary condition, other papers have explored methods of modeling the flow and temperature in and near supply air diffusers for inclusion into room CFD models (Huo *et al.*, 2000; Zhao *et al.*, 2003, 2006; Koskela, 2004; Einberg *et al.*, 2005).

Although recent research has attended to air inlet boundaries in enclosed spaces, relatively little work has focused on specifying the equally critical conditions of source boundaries, the surfaces and openings through which contaminants enter the computational domain. The purpose of this research was to demonstrate the importance of realistic and accurate characterization of source boundary conditions by comparing CFD concentration estimates with air sampling results. While air sampling is rightly considered to be the 'standard' of comparison, it is not error free. The presence of uncertainty in both tested and standard methods is a challenge to the validation of CFD for estimating potential exposure. Although the detailed treatment of uncertainty differs between these methods, some similarity is revealed by considering the treatment of uncertainty in method development and in method application. The development stage of CFD, including checking for errors in coding and in numerical solution of partial differential equations, and possibly eliminating them, is called 'verification'. Uncertainties also arise in the application of verified CFD methods, some of which are usually evaluated by end users, for instance, agreement between the conceptual model and the computational methods, grid adequacy, order of solution, conservation of mass, energy and momentum, and convergence (Roache, 1997). Then, the CFD results are compared with experimental or field observations, to complete the 'validation'.

Air sampling and analysis in occupational hygiene often begin with method development and the assessment of its accuracy. Methods and vocabulary of these methods have undergone significant changes in recent years (Bartley and Liden, 2008). Like CFD, considerable emphasis is placed upon uncertainty

during method development: the use of methods evaluated for workplace sampling helps determine uncertainty and confidence limits of measured values. Regarding CFD, Roach (1997) stated that 'useful *a priori* estimation of uncertainty is not possible for nontrivial fluid mechanics problems'. By this, he means that no CFD method can be validated for every possible circumstance of use. Likewise, the error of even most thoroughly evaluated sampling and analytical method could exceed the limits encountered in laboratory testing when used in some work settings.

Here, validation data from a capacitor manufacturing work area were collected and the distribution of isoamyl acetate (IAA) was simulated using CFD throughout the work area. The specific tasks were (i) to survey air velocity and airborne contaminant concentration at various locations in a work area; (ii) to define boundary conditions, including air vent velocity, source emission rates, and solid objects to be used in CFD simulation; and (iii) to simulate airflow and contaminant distribution in this area using CFD and compare CFD results with observed concentrations.

METHODS

Overview

Task 1, a workplace survey, was carried out in a facility that manufactures tantalum capacitors. The potential exposures resulted from the coating of capacitors with 'silver ink', a suspension of silver in a polymeric binder using IAA as a solvent, and the subsequent drying of coated batches of capacitors. The coordinates of all process equipment were determined on a 3-dimensional (3-D) grid within the work area and the locations of required measurement sites were planned in advance. On three subsequent days, air samples for IAA were collected using diffusive samplers and active samplers at locations distributed around the work area with a particular focus on the area near the IAA source. By comparing diffusive measurements with active sampling results, the application of diffusive samplers for area sampling in this work area was validated. Air velocities were also measured.

In Task 2, the data were analyzed to extract information needed to set up a CFD simulation of workroom airflow pattern and IAA distribution, including the boundary conditions. The computational domain was taken to be a rectangular box encompassing the entire 'silver dip area' excluding duct work and other solid objects. The boundary of this domain consisted of the following surfaces: the contaminant source, the supply air vents, the air exhaust vents, the floor, the ceiling, the three solid walls (including closed doors), and a 'pressure wall'. (The pressure wall was an open area between two zones—the computational domain and the rest of the room. Airflow through the pressure wall was a function of the pressure difference between these two zones.) Standard approaches were used for characterizing the solid boundaries. Air vent boundary conditions were established by measuring air speed at each vent. The other boundary conditions required more analysis as described below.

Task 3 consisted of the simulation of air movement and contaminant distribution in the work area using CFD. Then, the CFD-estimated air velocities and IAA concentrations were compared with measured values.

Task 1. Work area survey

The work area studied was the silver dip area in a capacitor manufacturing facility. It was located in the western end of a large room measuring 19.2 m (length) × 9.14 m (width) × 4.27 m (height). Supply air entered the large room through a rectangular duct, running the length of the room at the ceiling level with four pairs of vents; each pair discharged horizontally from opposite sides of the duct and the pairs were evenly distributed along its length. During this study, no manufacturing activities occurred in the eastern two-thirds of the room. Thus, air monitoring and CFD simulation was confined to the silver dip area, which measured 6.95 m (length) × 9.14 m (width) × 4.27 m (height) (see Fig. 1). Only the dipping station 'E-1' and the drying station 'E-2' were in use during this study.

In the portion of the manufacturing process studied, batches of tantalum 'slugs', previously coated with manganese dioxide and graphite, were suspended from movable racks and dipped into 'silver ink'. The dipping process was performed inside a laboratory hood and lasted ∼30 min per batch. Each batch was then moved to a cart (see Fig. 2), centrally located in the work area, for visual inspection, and then placed in the vented drying hood. This study was performed over three full work shifts on separate days, with production rates of 10, 24, and 14 batches per shift.

Temperature and humidity were monitored throughout the sampling periods with three indoor air quality instruments (IAQ Calc; TSI Inc., St. Paul, MN, USA). Two were placed inside the workroom, and the other was placed outside of the building, near the supply intake, to determine background conditions. In

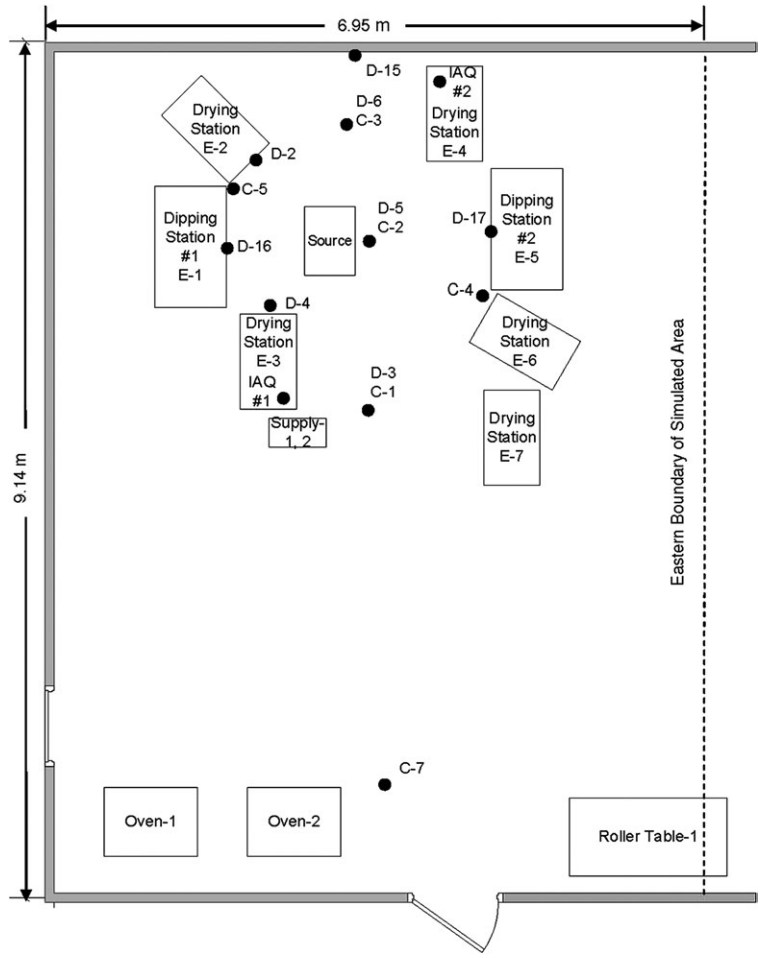

Fig. 1. The silver ink dip work area in a tantalum capacitor manufacturing facility studied in this research [6.95 m (L) × 9.14 m (W) × 4.27 m (H)], showing locations of monitoring devices: diffusive samplers (D), active charcoal tube samplers (C), and temperature/humidity/CO_2 (IAQ). Air exhausts (E) are also shown.

addition, air speed and direction were determined at various points around the capacitor rack. Air speed was measured using a thermoanemometer (Compu-Flow 8585; Alnor, Shoreview, MN, USA) and direction was determined using a smoke tube tracer.

For each work shift, 16 diffusive samplers (Chemdisk; Assay Technologies, Pleasanton, CA, USA for volatile organic compounds with a manufacturer-determined sampling rate for IAA of 6.58 cm^3 min^{-1} and a detection limit of 0.1 p.p.m. were used to collect full-shift exposures. To check that the actual sampling rates of the stationary diffusive samplers did not deviate from the rates given by the manufacturer, seven 50/100 charcoal tube area samples were collected along side some of the diffusive samplers using low flow personal air pumps (224-PCXR8 and Pocket Pump 210 Series; SKC Inc., Eighty Four, PA. USA) according to NIOSH Method 1450. The number of charcoal tube samples collected during a shift depended upon the production rate. Figure 1 shows the locations of diffusive samplers (D), charcoal tubes (C), and the temperature/humidity instruments (IAQ). A close-up drawing of the source area is shown in Fig. 3. The diffusive samplers were analyzed by Assay Technologies and the charcoal tubes from the active sampling were analyzed by the industrial hygiene laboratory at US Navy Environmental and Preventive Medicine Unit #2 (Norfolk, VA, USA).

In addition, diffusive samplers were placed on two workers in the silver dip area as personal monitors. The work tasks of these workers was to move batches of capacitors into the dip area, through the

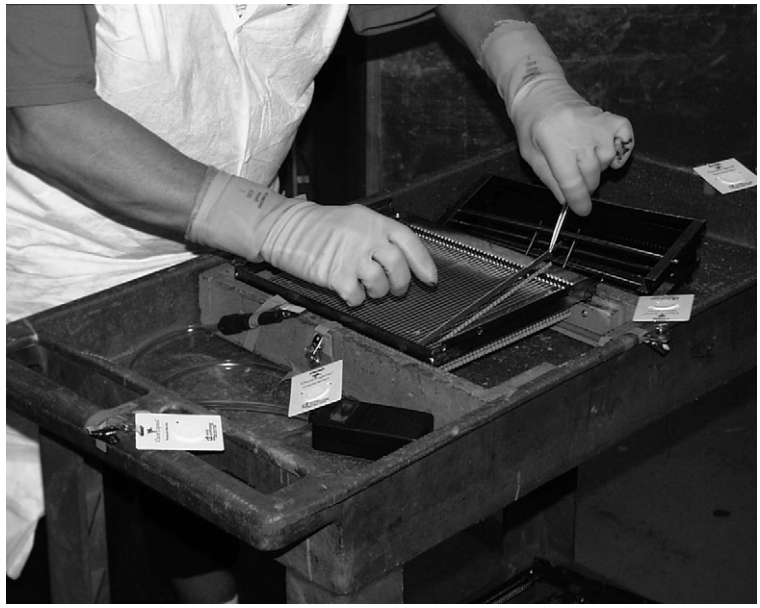

Fig. 2. Picture of capacitor inspection cart.

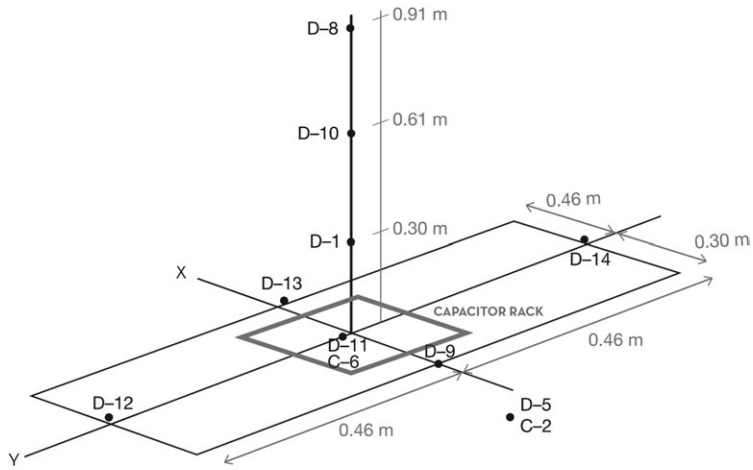

Fig. 3. Schematic close-up of source area showing sampling locations.

processing stations, and out of the room after several hours of drying. They wore protective gloves and aprons but no respiratory protection: the levels of IAA measured by personal sampling were well below the US Occupational Safety and Health Administration's standard and the American Conference of Governmental Industrial Hygienists' Threshold Limit Value.

Task 2. Boundary conditions

Air inlet boundary conditions. Recognizing the importance of inlet air boundary conditions as discussed above, all the supply vents were carefully characterized. Each of the eight supply vents measured 0.3 (H) × 0.6 m (W) with 16 horizontal and 31 vertical vanes and blew a jet of air along the ceiling perpendicular to the duct. The face of each vent was divided into 12 equal area zones, and air speed was measured at the center of each zone.

Only two of the eight supply air vents, but all the exhaust openings, were located in the work area to be simulated—the silver dip area—resulting in a general flow of air from the eastern end of the room into the dip area. The eastern boundary of the simulated

space was taken to be a 'pressure wall', a plane dividing the dip area from the rest of the room. The flow rate through this plane was controlled by the pressure difference between these two workroom zones.

The exhaust systems in the large workroom, which includes the silver dip area, consisted of 4 lab hoods, 12 drying hoods, and a floor level exhaust at the end of the exhaust duct. Outside the room, but attached to the same exhaust system, there was a silver ink quality assurance lab hood and a reclamation cabinet in which sponges that had been used in the dipping process were stored.

Inside the dipping work area, the exhaust system comprises seven branches—two dip stations and five drying stations—attached to a large duct which acted as a plenum. The dipping equipment, including a tank containing silver ink and a mechanism for lowering and raising the capacitor racks, is enclosed in a laboratory hood with a 1.5 m (W) $\times$ 0.36 m (H) open face. The drying station was a ventilated aluminum enclosure with a door in the lower front allowing carts holding multiple batches of capacitors to the wheeled in and out; the upper front was a 0.6 m (W) $\times$ 0.9 m (H) opening.

Direct and accurate measurement of the flow rates in these exhaust branches was not practical in this facility. Therefore, the flow rates in all branches were determined using simultaneous solution of a system of algebraic equations relating branch pressure drop to airflow rates given the following constraints: (i) the static pressure drops for all the seven branches were equal because all branches of the system were attached to the same large main duct, which had little pressure drop and thus relatively uniform static pressure (ACGIH Ventilation Committee, 2004); (ii) all five drying stations had the same flow rate set using blast gates; (iii) both lab hoods have the same flow rate; (iv) the total exhaust flow rate measured in a stack on the roof was equal to the sum of the individual branch flow rates. This calculation showed that the flow rate from each drying station was 0.344 $m^3\ s^{-1}$ (face velocity = 2.6 m min^{-1}). The flow rate from each lab hood was 0.774 $m^3\ s^{-1}$ (face velocity = 280 m min^{-1}), and the static pressure drop across all branches was 324 pa. Thus, the total exhaust flow from the work area studied was 3.27 $m^3\ s^{-1}$, remarkably close to the independently measured supply airflow rate of 3.23 $m^3\ s^{-1}$.

Based upon the difference between the supply and exhaust flow rates for the dip area, the flow rate from the eastern end of the room was determined. This was used to calculate the pressure-wall boundary condition, an air velocity of 0.055 m s^{-1} (flow rate/area of the pressure wall) from east to west. Because this velocity was rather low and none of the supply jets blew toward the pressure wall, the velocity across the pressure wall was assumed to be uniform.

Source boundary conditions. A critical feature of the source boundary condition is the IAA emission rate. This rate was calculated from a mass balance on IAA in the 'near field', a hemispheric volume similar to that used in the 2-zone model for exposure analysis (Hemeon, 1963; Heinsohn, 1991; Nicas, 1996). The near field was centered on the source and had a radius of 0.46 m. The rest of the silver ink area was called the 'far field'.

IAA emissions rates are highest when a batch of capacitors is removed from the dip station and placed on the inspection cart (Fig. 2). Emissions then diminish as the capacitor coating continues to dry. Over numerous batches, the time-weighted average (TWA) emission rate, G, approximates the TWA rate of convective transport out of the near field minus the TWA rate of convective transport into the near field from the far field. Like the two-zone model, the TWA rate of convective transport out of the near field was equated to the near-field concentration, C_N, times the rate of gas exchange, β, between the near and far fields. Unlike many applications of the two-zone model, the mean of the six TWA concentrations in the near field was used as C_N: one measured concentration would not suffice because of the concentration gradient. Another modification of the two-zone model was used because the far field was not well mixed. Thus, the TWA rate of convective transport of IAA into the near field was calculated as the upwind TWA concentration closest to the near field, C_U (measured at location D-5, Figs 1 and 3), times β. Solving the modified model equation for G gave the following:

$$G = C_N\beta - C_U\beta. \quad (1)$$

The wind direction near the source was found with smoke tubes to be essentially east to west and parallel to the floor. The average air speed upwind of the near field was obtained from a series of thermoanemometer readings. Then, β was calculated by multiplying the average upwind air speed times the cross-sectional area of the near field. The average G for a work shift was calculated separately for each of the 3 days because the production rate varied from day to day.

After determining the IAA emission rates, it was necessary to translate them into CFD boundary conditions for the source. CFD simulations of the transport of contaminants in enclosed spaces often

require assumptions that have not been previously tested. Here, as a first approximation, a flat surface across the top of the rack holding rows of capacitors at the inspection station (Fig. 2) was used as the source boundary and the emission through that surface was represented as diffusive flux of IAA molecules into the flowing air stream above the surface, such that the total emission rate equaled G.

Solid boundary conditions. For solid boundaries, the standard wall function built into Fluent was used assuming no slip, smooth surfaces, and no diffusive flux of species.

Task 3. CFD simulation

The first step in the simulation was to divide the solution space into numerous cells, each of which serves as a control volume. The dipping area was modeled in 3-D using Gambit 2.0 (Fluent Inc., Lebanon, NH, USA) with a mesh of tetrahedral cells to accommodate the geometry of the hoods, drying racks, and tables. All boundary conditions were constant except for the emission rates, which were different for each of the 3 days studied.

A segregated solver of finite difference-based CFD (Fluent 6.1.22; Fluent Inc.) was used to solve the system of governing equations—continuity, momentum, and species transport. The solution was found for isothermal conditions because the room temperature was kept constant for process control and all solid room boundaries are interior walls.

Like all deterministic models, the application of CFD requires some assumptions. One such assumption was the use of TWA emission rates paired with steady-state CFD to estimate the TWA concentrations. The rationale for doing is the following. (i) The IAA emissions to workroom air occurred in a repeating cycle: starting with removal of a batch of capacitors from the dipping workstation, decreasing through the inspection process, dropping to zero when placed in the ventilated drying station, and beginning again with the next batch. The concentration versus time for repeated cycles of emissions into a well-mixed isothermal ventilated space was simulated using a spreadsheet. The TWA concentration, C_{TWA}, over an integral number of complete cycles was found to be equal to a steady-state solution ($C_{TWA} = G_{TWA}/Q$) using the TWA emission rate, G_{TWA}. (ii) In the dipping area, the emission rate varies with time. Our previous work with steady-state CFD has shown that the estimated concentration at each grid point throughout an enclosed space is directly proportional to the emission rate, provided that the emission occurs at a sufficiently low rate that it does not disturb the room airflow pattern (Feigley *et al.*, 2002). The emission rate and velocity from capacitors on the inspection table were thought to be sufficiently low. Thus, the combination of these two observations led us to be believe that the use of the TWA emission rate with steady-state CFD was warranted.

The standard two-equation k-ε turbulence model at a steady state was chosen to model turbulence due to its simplicity and applicability for the flow under consideration.

For discretization, (i) the body force weight scheme was chosen for pressure-velocity coupling, (ii) a first-order upwinding scheme was used for momentum, turbulence, and species governing equations, and (iii) under-relaxation factors were manipulated to get quicker convergence and the solution was assumed to converge when the residual for all scalars were $\leq 1.0 \times 10^{-6}$.

Grid independence was tested by comparing results of the original number of cells (120K) with results of an increased number of cells (295K). The grid average difference in velocity was relatively small (0.17%). The final simulations were performed using 295K cells.

Simulation 1. Results from Simulation 1 suggested that diffusion of pure IAA vapor through the flat plane did not adequately represent the dilution achieved when the vapor was released from numerous coated capacitors with air flowing among these small sources. In a previous study, the solvent loss rates during the drying of similar polymer coatings (e.g. paints) were measured at various times within 20 min after application to a flat surface (Feigley *et al.*, 1981). Solvent emission rates began to decrease within the first minute or 2. Because air boundary layer conditions were constant, the decreasing loss rate was attributed to increasing mass transfer resistance within the polymer coating. As the solvent in the coating near the air interface was depleted, the diffusion coefficient of the solvent in the polymer decreased. This was attributed to the diminished spacing between polymer molecules. For a solvent that was 84 mole % ethanol, the time required for 90% of the ethanol to leave the coating ranged from 4 to 13 min, depending upon the air velocities studied. After this initial 'wet' stage, the rate of loss changed very little and was independent of air velocity.

In the capacitor coating process studied here, batches of capacitors were allowed to dry for ~20 min before they were moved to the inspection station. The rate of IAA permeation out of the coating would have slowed significantly. Therefore, vapor concentration at the coating-air interface would

be well below the vapor concentration at the surface of pure IAA liquid and would continue to decrease during the visual inspection of the capacitors. Due to the complexity of the drying process, estimating the emission rates, from basic principles, of an array of capacitors as a function of time would be extremely challenging. The rate from each individual capacitor would likely vary with position on the surface of the coated capacitor. The solvent diffusion coefficient within the polymeric coating is a function of the local IAA concentration and local temperature; both IAA concentration and temperature vary with time and location within the coating. Thus, the measured IAA concentrations were used directly to obtain a more realistic boundary condition for a second set of simulations.

Simulation 2. The next set of simulations was performed using the same rates of IAA emission as the first set, but the emission consisted of IAA diluted in the air to a level consistent with the nearest measured concentrations (56 p.p.m.). This is a more realistic representation of the source: on a molecular scale, individual molecules of IAA would have diffused out of the coating at a rate much slower than the loss rate from the surface of pure liquid IAA. Entering the air stream flowing past each capacitor, the IAA vapor would have been immediately diluted, even at the coating surface.

Analysis. Paired velocity or concentration results obtained by different methods were first compared graphically and by computing the Pearson correlation coefficient (r). Because relatively few data points were available for these comparisons, several of the common tests for normality were not applicable. Characteristics of the distributions were assessed by plotting histograms and testing the statistical significance of the skewness and kurtosis of these distributions using the approximate method described by Tabachnick and Fidell (1996). When evidence of non-normality was found, the data were logarithmically transformed and normality tested again. Finally, the means of the two transformed results were compared using a two-tailed paired t-test.

RESULTS AND DISCUSSION

Comparison of IAA concentrations between diffusive and charcoal tube samplers

At the work area locations where both diffusive and charcoal tubes samples were collected, concentrations measured by diffusive samplers were found to agree well with concentrations measured by charcoal tubes (Fig. 4). Combining monitoring results over all 3 days, the Pearson correlation coefficient was 0.97. A paired t-test showed no evidence of a significant difference in the means of the two monitoring methods ($P = 0.36$). Given this good agreement and the larger number of locations monitored with diffusive samplers, the diffusive sampling results were employed in the subsequent analyses.

Estimation of source generation rates for both simulations

Air speeds measured near the source are shown in Fig. 5. The mean air speeds measured at six points in the near field (0.284 m s^{-1}) times the cross-sectional area of a hemisphere enclosing the capacitor rack (0.328 m^2) yielded a β of 0.093 m^3 s^{-1}, which represents the air exchange rate between the near and far fields. Equation 1 was then used to estimate the emission rate. The average near-field concentration, C_N, was calculated separately for each day (9.6, 24,

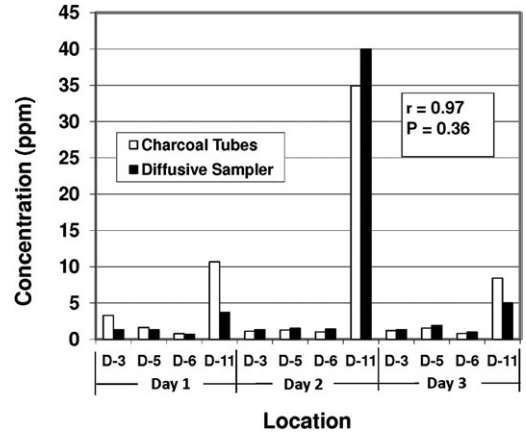

Fig. 4. Comparison of IAA concentrations measured by diffusive sampler versus charcoal tube samplers at four locations (D-3/C-1, D-5/C-2, D-6/C-3, and D-11/C-6) over 3 days.

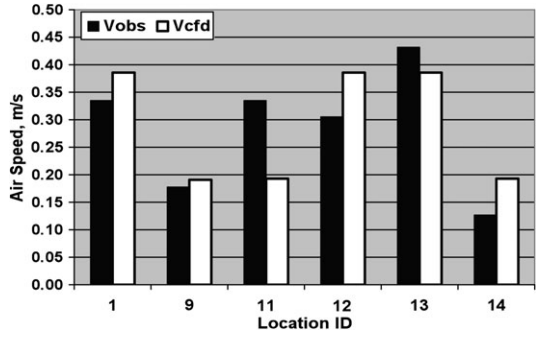

Fig. 5. Comparison of room air speed estimated by CFD with air speed measured by thermoanemometer (m s^{-1}) at six locations near the isoamyl acetate source.

11 p.p.m.) by averaging concentrations at six locations (D-1, 9, 11, 12, 13, and 14—see Fig. 3). The measured upwind concentration (at location D-5) was used for C_F (1.3, 1.5, 1.9 p.p.m.) for each day. The resulting emission rates, number of capacitor batches manufactured, and the emission factors for each day are shown in Table 1. Numerous factors may influence emission rate estimates, including those that actually change the emission rates and those that cause errors in the estimates. The emission rates for the 3 days studied have a relative standard deviation (RSD) of 59%. However, normalizing by the number of batches produced an emission factor with an RSD of 18%. This level of agreement among the three days adds confidence to the emission rate estimates.

Air velocities

In Simulation 1, the ability to model airflow patterns was evaluated by comparing observed and CFD-estimated air velocity at the six locations where it had been measured. The Pearson correlation coefficient was 0.70 and the paired *t*-test revealed no significant difference between the estimated and measured air speeds (P= 0.92), but the small sample size suggests relatively low statistical power for detecting differences between the methods. Figure 5 also shows reasonably good agreement; the poorest match was at point D-11, the point closest to the center of inspection table. The CFD-estimated direction of airflow qualitatively agreed with smoke tracer determinations.

IAA concentrations

The principal measure of how well CFD performs is the degree of agreement between CFD-estimated contaminant concentrations and concentrations determined by air sampling. This validation attempt for the first set of simulations (i.e., when the source was assumed to emit pure IAA) showed large concentration differences between the two estimation methods, despite the reasonably good match obtained for air velocities. Closer examination of the CFD results indicated that the most concentrated portions of the IAA plume were predicted to stay close to the inspection table surface. Furthermore, part of the plume carried over the table edge and settled toward the floor. This is likely due to limited dilution near the source and the fact that the emissions were represented as pure IAA vapor, which would have been 4.48 times as dense as the surrounding air. This suggested that the representation of the source boundary condition was in error.

As mentioned in the Methods section, reflection on the nature of the source indicated that the emission was not pure IAA, even at the surface of the capacitors. IAA would have permeated slowly through a layer of drying coating material on each of the many tiny capacitors and thus was emitted in a dilute form. It was then diluted further by passing air. Therefore, a more realistic source model was needed. In the second set of simulations, the same IAA emission rates were used, but the source was represented as a release of a mixture of IAA and air, resulting in an initial plume density of less than 1.0003 times that of the surrounding air.

The results of CFD simulation using a dilute IAA emission are compared with measured concentrations on a point-by-point basis in Fig. 6. The results correlate relatively well: the Pearson correlation coefficient is 0.74. The largest differences between the means were observed for samples D9, D13 and D14, but a paired *t*-test on log-transformed variables found no statistically significant difference between the means of CFD concentrations and those of the measured concentrations (P = 0.67). The error bars in Fig. 6, which represent plus or minus one standard deviation, are influenced by the variation in the

Table 1. Isoamyl acetate emission rate (G), number of batches manufactured (N), and emission factor (E) by day; E = G/N

Day	Emission rate (mg s^{-1})	Number of batches (batches)	Emission factor (mg s^{-1} $batch^{-1}$)
1	4.1	10	0.41
2	11.1	24	0.46
3	4.5	14	0.32

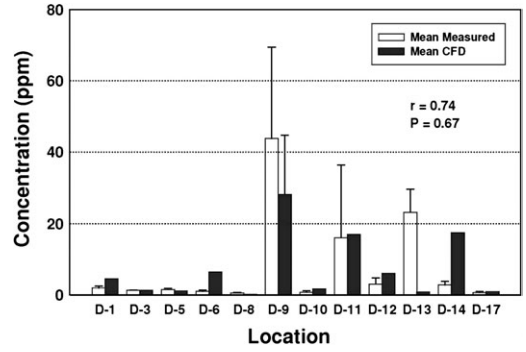

Fig. 6. Comparison of mean IAA concentrations estimated by steady-state CFD using a dilute source with mean 8-h (IAA) concentration measured by diffusive samplers (p.p.m.) at 12 work area locations. Concentrations are shown as means of three daily concentration values at each location with the corresponding standard deviations as error bars.

emission rate, process and environmental conditions, and measurement error.

To assess the impact of emission rate on the CFD concentrations, the concentration values were normalized by dividing them by the daily emission rates. Then, the RSD (RSD = SD per mean) was calculated separately for each monitoring location. The median RSD for normalized CFD concentrations across all 12 locations was 4 versus 59% RSD for raw CFD concentrations. This agrees with the relationship between concentrations and emission rates found in previous simulations of contaminant distribution in a workroom (Feigley *et al.*, 2002). Thus, most of the day-to-day variability in CFD concentration was thought to result from changes in the emission rate, which in turn was related to the production rate in batches per shift.

In addition to comparison of measured and CFD mean concentrations on a paired basis, comparison of means in the near field, far field, and throughout the room were also of interest (Table 2). The analyses above demonstrated good agreement between measured and CFD concentrations averaged over all measurement locations. Here, CFD concentrations averaged at measurement locations and over all CFD nodes are shown to agree relatively well with the mean of the measurements in the source near field and in the far field. Also, the mean measured exposure levels obtained with diffusive samplers in the workers' breathing zone were slightly higher than the mean of the far-field CFD concentrations, while lower than the near-field values. These values seemed reasonable because the workers spend most of their time in the far field and are only in close proximity to the source when inspecting batches of capacitors.

Table 2. Mean steady-state CFD-estimated concentrations at nodes in the near field and far field compared with mean measured concentrations at fixed locations in each field and mean personal exposure levels[a]

	At measurement locations			At all nodes	
	N	Measured (p.p.m.)	CFD (p.p.m.)	*N*	CFD (p.p.m.)
Near field (≤0.46 m from source center)	21	13.1	10.9	442	11.0
Far field (>0.46 m from source center)	15	1.0	2.0	197,973	1.2
Personal samples	6	2.2	—	—	—

[a]Means calculated over all 3 days combined (Simulation 2).

The effects of other boundary conditions on airflow patterns also have been observed far into rooms. For instance, energy may be concentrated at a wall with a measurable temperature difference; this can affect airflow and contaminant dispersion in the room through natural convection and radiation (Angioletti *et al.*, 2003; Teodosiu *et al.*, 2003; Srebric *et al.*, 2008). Contaminant concentration is highest near the contaminant source and source characteristics can have a significant impact on patterns of contaminant distribution, as shown here. Little research has been performed on source boundary effects in rooms and studies in this area have been primarily limited to the determination of emission rates and emission factors. As demonstrated here, some additional information on density of emissions and the near-field airflow patterns may be needed to achieve accurate simulation of contaminant distribution.

CONCLUSIONS

CFD simulation of a 'silver ink' work area in a capacitor production process was able to predict accurately the air velocity patterns near the inspection table based on carefully characterized air inlet and outlet vents. When we assumed that pure isoamyl acetate (IAA) vapor was released from the capacitor coating, concentration estimates did not agree well with measured concentrations. After adjusting the source boundary characteristics to more realistically represent IAA emissions, the difference between the measured concentrations and the CFD concentrations were not statistically significant.

Momentum is highly concentrated at room air inlets; likewise, contaminants are highly concentrated near sources. Thus, the CFD solutions are very sensitive to the representation of air inlet and source boundary conditions. Unrealistic and simplistic assumptions at inlet boundaries can produce extreme errors in CFD results throughout a room. This study demonstrates that, if sufficient attention is paid to assessing relevant boundary conditions, CFD simulation can yield results that agree well with measured values.

The sampling survey for this project was intended to provide adequate data for validating methods for estimating concentrations using CFD; thus, it was more extensive than most occupational hygiene field surveys, especially in the source's near field and at the supply air vents. To more easily apply CFD in occupational settings, further research is needed to determine how best to characterize boundary conditions. Several studies modeled the distribution of air

from supply vents (for example Huo *et al.*, 2000; Koskela, 2004; Einberg *et al.*, 2005); such models may reduce the amount of data collection necessary for establishing air inlet boundary conditions. As a complement to development of models for exposure analysis, research is needed to establish methods and instrumentation for characterizing contaminant sources. Although some methods have been developed to estimate emission rates, they often require sizable expenditures of time and money. The extent of CFD use for exposure estimation and control in the future will depend upon the availability of accurate rapid approaches for assessing source boundary conditions.

FUNDING

United States National Institute for Occupational Safety and Health, Centers for Disease Control and Prevention (R01 OH07626) to C.F.

REFERENCES

ACGIH Ventilation Committee. (2004) Industrial Ventilation: A Manual of Recommended Practice. 25th edn. Cincinnati, OH, USA: American Conference of Governmental Industrial Hygienists.

Anderson DA, Tannehill JC, Pletcher RH. (1984) Computational Fluid Mechanics and Heat Transfer. Philadelphia, PA: Taylor and Francis.

Angioletti M, Di Tommaso RM, Nino E *et al*. (2003) Flow field analysis in a ventilated large enclosure subject to non-homogeneous boundary conditions. Heat Transfer Eng; 24: 42–56.

Bartley D, Lidén G. (2008) Measurement uncertainty. Ann Occup Hyg; 52: 413–7.

Bennett JS, Feigley CE, Khan J. (2003) Comparison of emission models with computational fluid dynamic simulation and a proposed model. Am Ind Hyg Assoc J; 64: 739–54.

Einberg G, Hagstrom K, Mustakallio P *et al*. (2005) CFD modelling of an industrial air diffuser—predicting velocity and temperature in the near zone. Build Environ; 40: 601–15.

Feigley CE, Bennett JS, Lee E *et al*. (2002) Improving the use of mixing factors for dilution ventilation design. Appl Occup Environ Hyg; 17: 333–43.

Feigley CE, Ehmke FM, Goodson TH *et al*. (1981) Experimental determination of volatile evolution rates from coated surfaces. Am Ind Hyg Assoc J; 42: 365–74.

Heinsohn RJ. (1991) Industrial ventilation engineering principles. New York, NY: John Wiley and Sons. pp. 264–71; b. p179–81.

Hemeon WCL. (1963) Plant and process ventilation. 2nd edn. New York, NY: Industrial Press Inc. pp. 235–45.

Huo Y, Haghighat F, Zhang JS *et al*. (2000) A systematic approach to describe the air terminal device in CFD simulation for room air distribution analysis. Build Environ; 35: 563–76.

Koskela H. (2004) Momentum source model for CFD-simulation of nozzle dust air diffuser. Energy Build; 36: 1011–20.

Lee E, Feigley CE. (2002) An investigation of air inlet velocity in simulating the dispersion of indoor contaminants via computational fluid dynamics. Ann Occup Hyg; 46: 701–12.

Nicas M. (1996) Estimating exposure intensity in an imperfectly mixed room. Am Ind Hygiene Assoc J; 57: 542–50.

Nielsen PV. (2004) Computational fluid dynamics and room air movement. Indoor Air; 14 (Suppl. 7): 134–43.

Patankar SV. (1980) Numerical heat transfer and fluid flow. Philadelphia, PA: Taylor and Francis.

Roache PJ. (1997) Quantification of uncertainty in computational fluid dynamics. Annu Rev Fluid Mech; 29: 123–60.

Sorensen DN, Nielsen PV. (2003) Quality control in computational fluid dynamics in indoor environments. Indoor Air; 13: 2–17.

Srebric J, Vukovic V, He G *et al*. (2008) CFD boundary conditions for contaminant dispersion, heat transfer and airflow simulations around human occupants in indoor environments. Build Environ; 43: 294–303.

Tabachnick BG, Fidell LS. (1996) Using multivariate statistics. 3rd edn. New York, NY: Harper Collins.

Teodosiu C, Rusaouen G, Hohota R. (2003) Influence of boundary conditions uncertainties on the simulation of ventilated enclosures. Numerical Heat Transfer, Part A; 44: 483–504.

Zhao B, Li X, Ren H *et al*. (2006) Air supply opening model of ceiling diffusers for numerical simulation of indoor air distribution under actual connected conditions, part I: model development. Numerical Heat Transfer, Part A; 50: 45–61.

Zhao B, Li X, Yan Q. (2003) A simplified system for indoor airflow simulation. Build Environ; 38: 543–52.